An enhanced SPH-based hydroelastic FSI solver with structural dynamic hourglass control

Yi Zhan, Min Luo*
Ocean College, Zhejiang University,
Zhoushan Zhejiang, China
min.luo@zju.edu.cn

Abbas Khayyer
Department of Civil and Earth Resources Engineering,
Kyoto University,
Kyoto, Japan

I. INTRODUCTION

The Total Lagrangian SPH (TLSPH) framework has been widely adopted in simulating fluid-structure interaction (FSI) problems due to its flexibility and robustness. However, the TLSPH framework still suffers from rank deficiency, or zero-energy modes, which typically manifests as non-physical zigzag particle distributions and/or unphysical particle clustering in particle-based structural models. These errors primarily arise from that the field variables and their derivatives are approximated at the same computational nodes, which are particles in SPH.

To address or mitigate the rank deficiency issue, several numerical methods have been proposed, such as introducing additional stress points, applying artificial viscosity terms, or employing Riemann stabilization terms. However, these algorithms introduce a certain level of algorithmic complexity or involve empirical and case-dependent coefficients. While they can suppress zero-energy modes, they often do not completely eliminate them, particularly in the presence of large deformations and imprecisely imposed boundary conditions, such as traction-free boundary conditions. An effective approach is adopting a corrective force/displacement-based hourglass mode control method [1]. This method evaluates the difference between the deformation predicted with the deformation gradient tensor and the actual deformation and combines the linear spring theory to calculate the artificial force term. This force term is then incorporated into the momentum equation to suppress the zero-energy modes. However, this method involves a constant coefficient α, which controls the magnitude of the corrective force and is case/resolution dependent and, hence, needs proper calibrations. A low α value may not suppress the hourglass mode sufficiently, while a high value causes the structure to become numerically over-stiffed, thereby affecting the reproduced kinematics and possibly resulting in instabilities. That is, for different cases and resolutions, the value of α needs to be calibrated and determined based on pre-simulations or experience.

To address the above issues, this study develops an advanced FSI solver based on the open-source code DualSPHysics+ [2]. The calculation of the structural domain is characterized by incorporation of three advanced schemes. Firstly, a Dynamic HourGlass Control (DHGC) scheme, is proposed to effectively suppress the zero-energy modes while being case- and resolution-independent. Secondly, a second-order consistent discretization of the deformation gradient tensor (F2nd) [3] is adopted to achieve second-order completeness and higher accuracy in the discretization of the structure governing equations. Thirdly, a tuning-free Riemann Stabilization (RS) term [4] is incorporated into the structural momentum equation to mitigate the rank deficiency issue and at the same time to improve numerical stability in presence of shocks and kinematical discontinuities. For the solving of the fluid domain, the Velocity divergence Error Mitigating (VEM) [5] and Hyperbolic/Parabolic Divergence Cleaning (HPDC) [6] schemes are incorporated into the SPH-based FSI simulations for the first time, which mitigate the errors in velocity divergence field and therefore the spurious fluid pressure noises resulting in enhanced hydroelastic FSI simulations.

II. NUMERICAL METHODS

A. FSI model

The governing equations for fluid can be discretized using the widely adopted δ-SPH [7,8] method as:

$$\frac{D\rho_i}{Dt} = -\rho_i \sum_j \boldsymbol{u}_{ij} \cdot \nabla_i W_{ij} V_j + D_i \tag{1}$$

$$\frac{D\boldsymbol{u}_i}{Dt} = -\sum_j m_j \left(\frac{p_i + p_j}{\rho_i \rho_j} \right) \nabla_i W_{ij} + \sum_j m_j \left(\frac{4\nu \boldsymbol{r}_{ij} \cdot \nabla_i W_{ij}}{(\rho_i + \rho_j)(r_{ij}^2 + \eta^2)} \right) \boldsymbol{u}_{ij} + \boldsymbol{g}_i \tag{2}$$

Meanwhile, the VEM [5] and HPDC [6] schemes are implemented to reduce the errors in velocity-divergence fields and thus, to achieve more accurate hydrodynamic pressure fields.

For the structure model, the momentum equation can be discretized with a second-order Taylor-series model as follows [3]:

$$\frac{D\boldsymbol{u}_i}{Dt} = \frac{1}{\rho_i^0} \sum_j \left(-\boldsymbol{P}_j \cdot \begin{bmatrix} \boldsymbol{A}_j^{0,1} \\ \boldsymbol{A}_j^{0,2} \end{bmatrix} \cdot \boldsymbol{M}_{ji}^0 + \boldsymbol{P}_i \cdot \begin{bmatrix} \boldsymbol{A}_i^{0,1} \\ \boldsymbol{A}_i^{0,2} \end{bmatrix} \cdot \boldsymbol{M}_{ij}^0 \right) \frac{\partial W_{ij}^0}{\partial r_{ij}^0} \frac{V_j^0}{\left| \boldsymbol{r}_{ij}^0 \right|} + \boldsymbol{\Pi}_i^{\mathrm{RS}} \tag{3}$$

where $\boldsymbol{P}$ is the first Piola-Kirchhoff stress tensor, $\boldsymbol{\Pi}_i^{RS}$ is a tuning-free Riemann stabilizing term [4], $\boldsymbol{r}_{ij} = (x_{ij}, y_{ij})$, $r = |\boldsymbol{r}|$, the matrix $\boldsymbol{M}$ and $\boldsymbol{A}$ are computed as:

$$\boldsymbol{M}_{ij}^0 = \left[\frac{x_{ij}^0}{\left| \boldsymbol{r}_{ij}^0 \right|} \quad \frac{y_{ij}^0}{\left| \boldsymbol{r}_{ij}^0 \right|} \quad \frac{1}{d_0} \frac{x_{ij}^0 x_{ij}^0}{\left| \boldsymbol{r}_{ij}^0 \right|} \quad \frac{1}{d_0} \frac{y_{ij}^0 y_{ij}^0}{\left| \boldsymbol{r}_{ij}^0 \right|} \quad \frac{1}{d_0} \frac{x_{ij}^0 y_{ij}^0}{\left| \boldsymbol{r}_{ij}^0 \right|} \right]^T \tag{4}$$

$$\boldsymbol{A}_i^0 = \left[\sum_j \boldsymbol{M}_{ij}^0 \otimes \boldsymbol{M}_{ij}^0 V_j^0 \frac{\partial W_{ij}^0}{\partial r_{ij}^0} \right]^{-1} \tag{5}$$

where d_0 denotes the initial particle spacing. The coupling between fluid and structure is modelled in a two-way weak coupling manner [9]. In each time step the fluid and structure are solved separately and one domain is treated as the boundary for the other.

B. *Dynamic hourglass control scheme*

In displacement-based hourglass control schemes, a numerical penalty force, denoted as $\boldsymbol{f}^{\mathrm{HG}}$, is introduced into the structural momentum equation. This force can be expressed as:

$$\boldsymbol{f}_i^{\mathrm{HG}} = -\frac{1}{2}\sum_j \frac{\alpha_i^k + \alpha_j^k}{2} \frac{V_{0i} V_{0j} W_{0ij}}{\left| \boldsymbol{r}_{ij}^0 \cdot \boldsymbol{r}_{ij}^0 \right|} \left(E_i \delta_{ij}^a + E_j \delta_{ji}^b \right) \frac{\boldsymbol{r}_{ij}}{\left| \boldsymbol{r}_{ij} \right|} \tag{6}$$

where $\boldsymbol{\epsilon}$ denotes the error vector between the local displacement vector and the linear transformation of the deformation gradient tensor. δ is the projection of the error vector $\boldsymbol{\epsilon}$ onto the position vector $\boldsymbol{r}_{\mathrm{ij}}$, computed as:

$$\delta_{ij}^i = \frac{\boldsymbol{\epsilon}_{ij}^i \cdot \boldsymbol{r}_{ij}}{r_{ij}} \text{ with } \boldsymbol{\epsilon}_{ij}^i = \left\langle \boldsymbol{r}_{ij} \right\rangle^i - \boldsymbol{r}_{ij} = \boldsymbol{F}_i \boldsymbol{r}_{ij}^0 - \boldsymbol{r}_{ij} \tag{7}$$

α is a dimensionless parameter that controls the magnitude of the penalty force. In DHGC, The value of α for a particle i is computed dynamically as the ratio of the magnitude of the error vector at the current time step to that at N time steps earlier, as:

$$\alpha_i^k = \left| \boldsymbol{\epsilon}_i \right|^k / \left| \boldsymbol{\epsilon}_i \right|^{k-N} \tag{8}$$

where the superscript k represents the current time step and N is adopted to be 50. α is initialized to be 1.0 and when the denominator approaches zero, α is capped at $\alpha_{max} = 50$. Sensitivity analyses are conducted for N and α_{max}, and investigations showed that results are insensitive to these selected values.

III. Numerical Investigations

Validations in terms of accuracy and efficiency are shown via classical benchmarks and experiments (e.g., [10,11]). Firstly, the rotation of an elastic square plate [10] is simulated to test the capability of the proposed schemes in simulating structural responses under continuous tensile stresses.

As shown in Figure 1(a), the simulation by F1st contains large errors and becomes unstable. The adoption of the second-order deformation gradient tensor (i.e., F2nd as shown in Figure 1(b)) achieves stable simulation, but the hourglass modes are evident, i.e., the nonphysical zigzag patterns in which pairs of particles interior of the plate move together and do not follow the rotation trajectory. By leveraging the developed DHGC scheme into the structural model as shown in Figure 1(c), the hourglass modes are significantly mitigated and the particles are generally evenly distributed. According to Figure 1(d), incorporation of the RS term effectively eliminates the pressure noises and achieves qualitatively accurate prediction of the pressure field. These results demonstrate that F2nd is superior to F1st in accuracy, DHGC effectively suppresses hourglass modes, and RS efficiently mitigates numerical noises. The combination of F2nd-DHGC-RS produces a more physically consistent pressure field and, hence, more accurate structural deformation prediction.

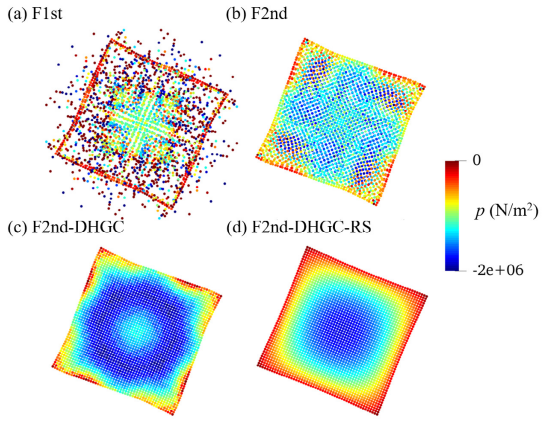

Figure 1. Snapshots of pressure contours at t = 0.15 s by F1st, F2nd, F2nd-DHGC and F2nd-DHGC-RS

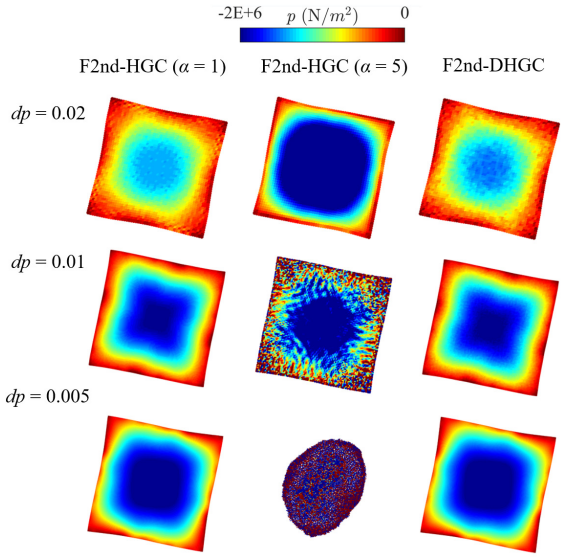

Figure 2. Snapshots of pressure contours at t = 0.29 s by F2nd-HGC (α = 1), F2nd-HGC (α = 5) and F2nd-DHGC

Simulations by different resolutions and different α values of the hourglass control scheme are conducted, and the pressure contours at t = 0.29 s (after several cycles of rotation) are presented in Figure 2. At the lower particle resolution (i.e., dp = 0.02), the plate deformation and pressure field predicted by F2nd (α = 1) and F2nd-DHGC are very close. With the refinement of particle spacing, the pressure fields produced by F2nd-HGC (α = 1) and F2nd-DHGC are enhanced in terms of reducing noises and both results are very close, while that by F2nd-HGC (α = 5) show noticeable unphysical fluctuations at dp = 0.01 and numerical instability at dp = 0.005. These comparisons show that DHGC effectively avoids the need for calibration of the parameter α at different resolutions as this coefficient is dynamically tuned based on the time evolution of an error function.

Figure 3 shows the time histories of the normalized mechanical energies with respect to the energy at the initial stage (i.e., E_{t0}) in the three simulations with dp = 0.01. The simulations by all the three scheme combinations show good energy conservation before t = 0.35 s. After that, the energy in the result by F2nd-HGC (α = 5) shows an unphysical rise, while that in F2nd-HGC (α = 1) result does not have this issue. The unphysical energy rise

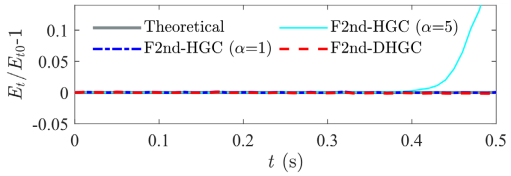

Figure 3. Time histories of normalized total mechanical energies in the system

is likely attributed to the kinematical instabilities associated with excessive hourglass control. As for the result by F2nd-DHGC, the energy is in good agreement with the theoretical solution.

Secondly, a dam break with an elastic plate [11] is simulated to verify the accuracy of the proposed FSI solver in simulating violent fluid-structure interaction. Figure 4 shows the predicted pressure and stress contours at t = 0.45 s together with the experimental photo. During the fluid impact on the elastic plate, violent pressures can be observed near the elastic plate. Such pressures are accompanied with significant fluid density variations due to the weakly compressible simulation framework as well as local kernel-based collocated approximations. Thus, the fluid experiences alternating compressions and expansions, manifested as acoustic pressure waves. In the F2nd-DHGC-RS result, the fluid pressure noises are evident and contaminate the entire fluid pressure field. These pressure noises further lead to inaccurate forces on the structure, ultimately resulting in noises in structural stresses. As shown in Figure 4 (c), such noises in the pressure and stress fields are effectively mitigated by the adoption of the VEM-HPDC schemes in the fluid model.

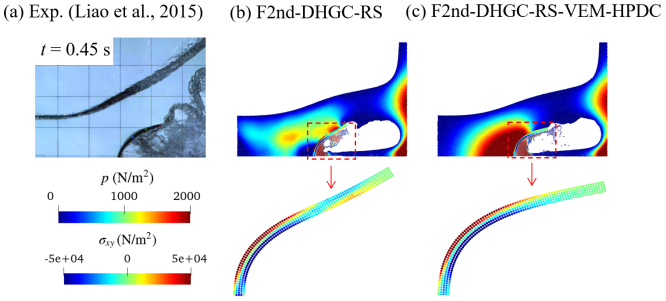

Figure 4. Snapshots of fluid and structure morphologies together with the stress/pressure fields along with experimental photos [11]

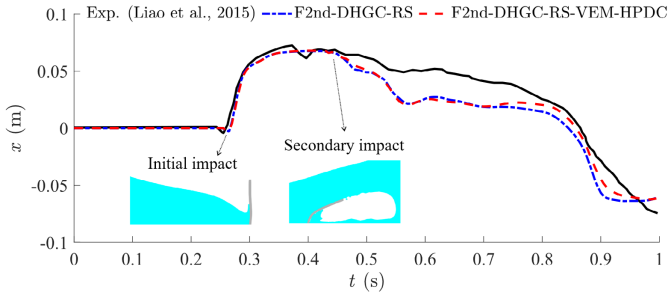

Figure 5. Time histories of the horizontal displacement of the plate's free end

The time histories of the horizontal displacement of the plate's free end are presented in Figure 5. The results by both models are in fairly good agreement with the experimental data. Specifically, a rebound of the plate occurs at t = 0.45 s due to the secondary impact of the reflected fluid. The model underestimates the rebound deflection amplitude due to the lack of air phase, further leading to the discrepancies between the predicted and experimental deflections from t = 0.45 s to 0.8 s. Despite this, the result by the model with VEM and HPDC is in a closer agreement with the experimental results.

IV. Conclusions

In this study, an enhanced structure model is developed and integrated with the recently published SPH open-source code DualSPHysics+ for free surface flows. The structural model is enhanced in three aspects. First, a novel DHGC scheme is proposed to mitigate the hourglass modes linked with the rank deficiency of TLSPH as a collocated computational method. The DHGC scheme adaptively adjusts the coefficient of hourglass controlling intensity based on the instantaneous state of error in the displacement field. This novel hourglass control scheme is case- and resolution-independent and effectively mitigates the rank deficiency issue of TLSPH in modelling large structural deformations. Second, a second-order discretization of the deformation gradient tensor is adopted, providing second-order completeness in solving the governing equations of structural dynamics. Third, a tuning-free Riemann diffusive term is incorporated into the momentum equation to mitigate spurious stress fluctuations. Regarding the fluid model, the VEM and HPDC are adopted to provide more accurate velocity divergence fields and thus noise-free pressure fields and, hence, enhance the modelling of fluid-structure interactions.

References

[1] G.C. Ganzenmüller, An hourglass control algorithm for Lagrangian Smooth Particle Hydrodynamics, Computer Methods in Applied Mechanics and Engineering. 286 (2015) 87–106.

[2] Y. Zhan, M. Luo, A. Khayyer, DualSPHysics+: An enhanced DualSPHysics with improvements in accuracy, energy conservation and resolution of the continuity equation, Computer Physics Communications. 306 (2025) 109389.

[3] A. Khayyer, Y. Shimizu, H. Gotoh, S. Hattori, A 3D SPH-based entirely Lagrangian meshfree hydroelastic FSI solver for anisotropic composite structures, Applied Mathematical Modelling. 112 (2022) 560–613.

[4] A. Khayyer, H. Gotoh, Y. Shimizu, T. Gotoh, An improved Riemann SPH-Hamiltonian SPH coupled solver for hydroelastic fluid-structure interactions, Engineering Analysis with Boundary Elements. 158 (2024) 332–355.

[5] A. Khayyer, Y. Shimizu, T. Gotoh, H. Gotoh, Enhanced resolution of the continuity equation in explicit weakly compressible SPH simulations of incompressible free-surface fluid flows, Applied Mathematical Modelling. 116 (2023) 84–121.

[6] G. Fourtakas, B.D. Rogers, R. Vacondio, An investigation on the divergence cleaning in weakly compressible SPH, in: Proceedings of the 17th International SPHERIC Workshop, Rhodes Island, Greece, 2023: pp. 55–62.

[7] M. Antuono, A. Colagrossi, S. Marrone, D. Molteni, Free-surface flows solved by means of SPH schemes with numerical diffusive terms, Computer Physics Communications. 181 (2010) 532–549.

[8] G. Fourtakas, J.M. Dominguez, R. Vacondio, B.D. Rogers, Local uniform stencil (LUST) boundary condition for arbitrary 3-D boundaries in parallel smoothed particle hydrodynamics (SPH) models, Computers & Fluids. 190 (2019) 346–361.

[9] J. O'Connor, B.D. Rogers, A fluid–structure interaction model for free-surface flows and flexible structures using smoothed particle hydrodynamics on a GPU, Journal of Fluids and Structures. 104 (2021) 103312.

[10] C.H. Lee, A.J. Gil, J. Bonet, Development of a cell centred upwind finite volume algorithm for a new conservation law formulation in structural dynamics, Computers & Structures. 118 (2013) 13–38.

[11] K.P. Liao, C.H. Hu, M. Sueyoshi, Free surface flow impacting on an elastic structure: Experiment versus numerical simulation, Applied Ocean Research. 50 (2015) 192–208.